A head loss based bridge module for TELEMAC-2D

Sebastian Gegenleithner[1], Clemens Dorfmann[2], Gabriele Harb[3], Josef Schneider[1]
s.gegenleithner@gmail.com, Graz, Austria
[1]: Institute of Hydraulic Engineering and Water Resources Management, Graz University of Technology
[2]: flow engineering, Graz, Austria
[3]: VERBUND Hydro Power GmbH, Vienna, Austria

***Abstract* – Capturing the backwater effects introduced by bridge structures is crucial for environmental flow studies. Hydrodynamic processes at these structures are inherently three-dimensional, particularly during high-flow stages when the bridge deck becomes submerged and pressurized flow occurs. Incorporating these effects into 2D depth-averaged models is not a straightforward task. One possible approach to approximate the three-dimensional effects is by computing the head losses exerted by the bridge on the flow and incorporating them as a source term in the momentum equation. In this contribution, we present a new head loss based bridge module for TELEMAC-2D that is based on Borda-Carnot expansion and contraction losses. The losses are computed in 1D, by utilizing the bridge's geometry and location as well as cross-sectional averages of velocities and free surface elevations. The resulting head losses are then directly applied as additional momentum sources, opposing the main flow direction at the vicinity of the bridge. The presented bridge module was validated with a comprehensive set of 176 experimental test cases. The results from the validation examples support the applicability and effectiveness of the presented approach.**

Keywords: Borda-Carnot, head loss, bridge modelling

I. INTRODUCTION

Bridge structures have a large influence on the overall runoff regime in free surface flows. Considering their effect is essential, especially in high flow conditions when the bridge deck gets submerged and pressurized flow occurs. In principle, the runoff at such structures can be divided into a total of three cases [1], which are schematically shown in Figure 1. The first case, Case 1 (blue line), occurs when the water level is far below the deck of the bridge and the runoff can be considered as free surface flow. For the second case, Case 2 (red lines), the upstream side of the bridge gets in contact with the water surface (section BU). Depending on the flow conditions, the downstream edge of the bridge (section BD) can be in contact with water (Case 2b, red solid line) or not (Case 2a, red dashed line). While in Case 2a a sluice gate type flow occurs, the flow for Case 2b is fully pressurized along the entire width of the bridge. For the third case (Case 3), the water level is above the upper edge of the bridge deck. For this case, the runoff is partly occurring as pressurized flow below the bridge deck and partly as free surface flow on the deck itself.

Modelling Case 1 in 2D depth-averaged models, such as TELEMAC-2D, can be easily done by considering the abutments and bridge piers geometrically in the mesh. This method allows for fully resolving the hydraulics of the bridge structure, e.g. the flow phenomena around the bridge piers. However, it falls short in capturing the additional increase in upstream water level when the bridge deck gets submerged.

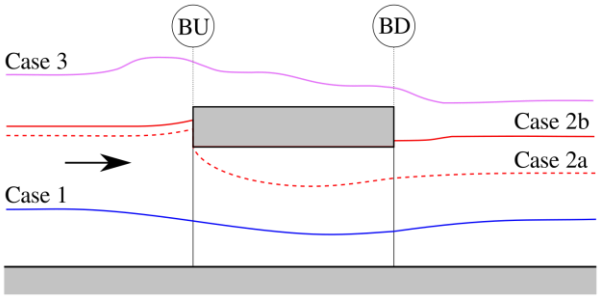

Figure 1. Schematic representation of water levels for different flow conditions at bridge structures. From [1] modified

For modelling the high flow conditions shown in Figure 1 (Case 2 and Case 3), several approaches can be found in literature. *HEC-RAS 2D* [2] computes the bridge flow by either solving the energy equation in 1D under consideration of contraction, expansion and friction losses or by computing the discharge through the structure by means of separate hydraulic equations for sluice gate flow (Case 2a), orifice flow (Case 2b) or a combination of weir flow and orifice flow (Case 3). The resulting difference in upstream and downstream water level is equated to a force, which is then applied in the momentum equation. *RiverFlow2D* [3] uses a modified Borda-Carnot approach to derive 1D contraction and expansion losses, which are applied as a head loss gradient in the momentum equation. In *Hydro_AS-2D,* bridges are modelled by means of the pressurized Saint Venant equations in combination with the weir flow equation for the overflow [4].

Approaches that are based on 1D hydraulic formulas, like weir flow, sluice gate type flow and orifice flow, are usually highly parameterized and thus the quality of the results strongly depends on the selected parameters for the application. In order to minimize the required user input, we settled for a similar method as it is used in *RiverFlow2D*, where the head loss formulation does not require any user defined parameters. Instead, the new bridge module solely requires a set of polylines, defining the locations and cross sections of the bridge structures.

II. METHODOLOGY

A. Modified subroutines and Keywords

The bridge module was implemented for TELEMAC version v8p4r0. Compiling the bridge module requires replacing and adding the files and subroutines listed in Table I. The subroutines can be obtained from the following GitHub repository: https://github.com/tuggegese/T2D_BridgeModule.

Table I Modified and added files required for compiling the bridge module

TELEMAC file	Changes/Implementations
bief_def.f	Added new vector structures
declarations_ telemac_2d.f	Added bridge relevant variables and allocatable containers
interface_telemac2d.f	Added new interface of the bridge module
lecdon_telemac2d.f	Added I/O operations for bridge keywords
telemac2d_init.f	Added call to the bridge routine "*bbuilder.f*"
deall_telemac2d.f	Added deallocation of bridge related variables
bbuilder.f	New subroutine that computes bridge parameters that do not change in time
prosou.f	Added the possibility to apply bridge head losses in each time step
telemac2d.dico	Added new variables
telemac2d.cmdf	Added new subroutine "bbuilder.f"
api.cmdf	Added new subroutine "bbuilder.f"

In order to model bridges in the study area, three additional keywords were added, namely:

- "NUMBER OF BRIDGES": Defines the total number of bridges in the study domain
- "BRIDGE LOCATION FILE": Links a file in .i2s format that contains all polylines defining the location of the bridges in the domain
- "BRIDGE SECTION FILE": Links a file in .i2s format containing closed polygons of all bridge cross sections

B. 1D Head loss formulation

Figure 2 presents a simplified sketch of a bridge with two abutments and a deck. The visualized flow conditions correspond to Case 2 in Figure 1. However, the hereafter presented methodology is thought to be valid for all cases. For the example case given in Figure 2, the head losses exerted by the bridge on the flow can be represented by summing the contraction losses between sections 1 and 2, the expansion losses between sections 3 and 4 and the friction losses between sections 1 and 4.

According to [5] and [6], the well-known Borda-Carnot expansion and contraction losses, that are commonly used to estimate energy losses due to sudden contractions and expansions in pipe flows, can be employed for free surface flows as well.

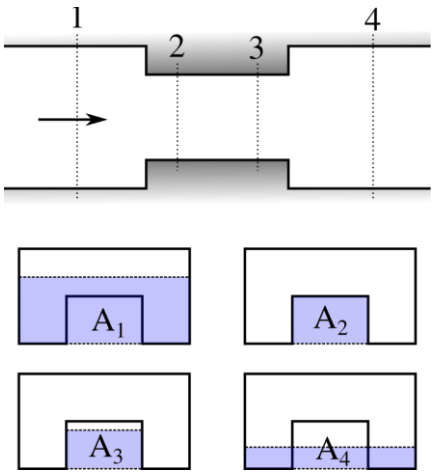

Figure 2. Schematic view of individual head loss components for cross sections 1 to 4

For the example bridge case, visualized in Figure 2, the Borda-Carnot expansion and contraction losses can be written as follows:

$$\Delta H_E = \frac{v_3^2}{2g}\left(1 - \frac{A_3}{A_4}\right)^2 \quad (1)$$

and

$$\Delta H_C = \frac{v_1^2}{2g}\left(\frac{1}{\mu} - 1\right)^2 \left(\frac{A_1}{A_2}\right) \quad (2)$$

where v_1 and v_3 are cross-sectional averages of the velocities upstream and below of the bridge. A_1 to A_4 are the cross-sectional areas covered by the flow and μ is the contraction coefficient, with typical values around 0.62 (see for example [5]). However, studies have shown (see for example [7]) that the contraction coefficient is not constant and is in fact dependent on several factors, such as the ratio of the downstream and upstream areas. For computing the contraction coefficient, we thus opted for the simplified approach of Weisbach, which can be written as follows:

$$\mu = c_1 + c_2 \left(\frac{A_2}{A_1}\right)^3 \quad (3)$$

with the coefficients c_1 and $c_2 = 1 - c_1$ being 0.63 and 0.37 [8], respectively. For the here presented implementation, we adjusted the parameters c_1 and c_2 trying to account for effects that influence the complex real-world energy losses, such as accelerations of the flow, deflections [7], the angle of the contraction or other 3D effects. By calibrating the later presented validation case, we have determined the coefficients to be $c_1 = 0.3$ and $c_2 = 0.7$. However, it has to be mentioned that the calibrated coefficients might not be optimal for all real-world examples and should be carefully assessed for each individual case.

The total losses of the bridge structure can be obtained by summing the individual components from contraction, expansion and friction, which can be expressed as:

$$\Delta H = \Delta H_C + \Delta H_E + \Delta H_F \quad (4)$$

In the current implementation, we have chosen to neglect the additional friction losses from the walls of the bridge. Consequently, the friction between sections 1 and 4 is solely determined by the bottom friction, potentially leading to slightly lower computed head losses compared to those occurring in nature.

C. *Implementing the head loss to the momentum equation*

The head loss exerted by the bridge structure on the flow can be added to the momentum equation as follows:

$$\frac{\partial u}{\partial t} = other\ terms - g\frac{\partial H}{\partial x} \quad (5)$$

$$\frac{\partial v}{\partial t} = other\ terms - g\frac{\partial H}{\partial y} \quad (6)$$

Where $\partial u/dt$ and $\partial v/dt$ are the local acceleration terms in x and y direction, $other\ terms$ include all not explicitly written terms, such as the gravitational acceleration, friction, diffusion, etc. and $\partial H/dx$ and $\partial H/dy$ are the derivatives of the local head loss.

For applying the head loss of a given bridge structure, we first have to define its location in the computational grid. The here presented implementation assumes that the entire head loss attributed to the bridge structure is acting on a number of cell edges, forming the cross section of the bridge (see Figure 3, purple line). At those edges, the total energy losses can be obtained by summing the head loss components from contraction, expansion and friction (Formula 4). The losses are constant for all element edges and are visualized in Figure 3 (Detail).

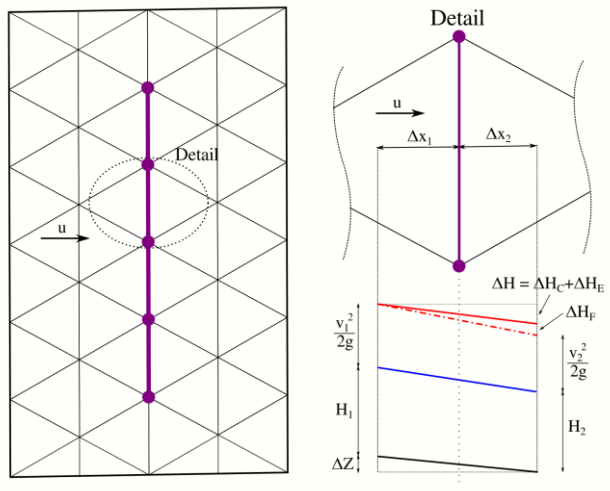

Figure 3. Scheme for computing head loss derivatives

Assuming that the head losses due to friction are solely introduced by bottom friction, which are already included in Equations 5 and 6, the additional head loss derivatives are composed of contraction and expansion only. Considering this as well as the fact that the head loss is always acting against the main direction of the flow, allows for computing the head loss derivatives with a cell centered finite difference scheme (shown for x direction only) as follows:

$$\frac{\partial H}{\partial x}_{CC} \approx \frac{\Delta H}{\Delta x_1 + \Delta x_2}\frac{u}{|u|} \quad (7)$$

where $\partial H/dx_{cc}$ is the head loss derivative computed by the cell centered scheme in x direction, ΔH is the head loss from contraction and expansion, $\Delta x_1 + \Delta x_2$ is the distances between the cell centers and $\partial u/|u|$ defines the directions of the head loss by taking a value of either -1 or 1 if the velocity is not zero. The compatibility with the node based formulation of TELEMAC-2D is reached by mapping the derivatives to the relevant nodes, effectively obtaining $\partial H/dx$.

D. *Detailed description of the algorithm*

The bridge module commences by initializing all static variables required for the analysis. Specifically, the two sets of polylines, given in the steering file are read. One file defines the bridge locations in the computational grid, and the other describes their respective cross sections (see Figure 4 dark blue lines). Assuming constant cross sections for both the bathymetry and the bridge structure along the entire width of the bridge, i.e. upstream geometry is equal to downstream geometry, enables the derivation of two functional relationships. The first links the free surface elevation to the unobstructed cross-sectional area just outside of the bridge, i.e. $A_{out} = f(FS)$. The second relationship connects the free surface elevation to the effective flow area of the bridge, considering the obstruction of the bridge structure, i.e. $A_{in} = f(FS)$.

Next, the algorithm identifies the set of nodes, referred to as nodestring, which closely matches the bridges specified location (Figure 4, blue line). Subsequently, the elements belonging to the nodestring are identified and the neighbouring nodes on both sides of the nodestring are extracted. Up to this point, the algorithm has no information which of the neighbouring nodes lie upstream and which lie downstream of the bridge. Since in environmental flow studies the flow might reverse, the choice which nodes lie upstream and which lie downstream is done in each time step in a later stage. Figure 4 gives an example for the upstream (red) and downstream (green) nodes for a given flow direction (black arrow). Additionally, the algorithm retrieves distances to the element centers (black line) required for computing the head loss derivatives (Formula 7)

After the initialisation step, head losses are computed and applied in each time step. The algorithm begins by calculating the average flux through the nodestring. Based on the present flow conditions, it determines which nodes lie upstream and downstream of the bridge. These nodes are then used to compute average free surface elevations, H_{US} and H_{DS}, respectively. Utilizing the previously derived functional relationships between free surface elevations and the areas below and outside, the algorithm determines the unobstructed and obstructed flow areas upstream and downstream of the bridge (see Figure 4). From the computed fluxes, cross sectional averages of flow velocities are obtained by applying the continuity equation. These velocities, along with the extracted flow areas, are used to derive the Borda-Carnot expansion (Formula 1) and contraction (Formula 2) losses, respectively. From those 1D losses, we are able to derive the head loss derivatives in x and y direction by using Formula 7 and apply them as additional terms in the momentum equation (Formula 5 and 6).

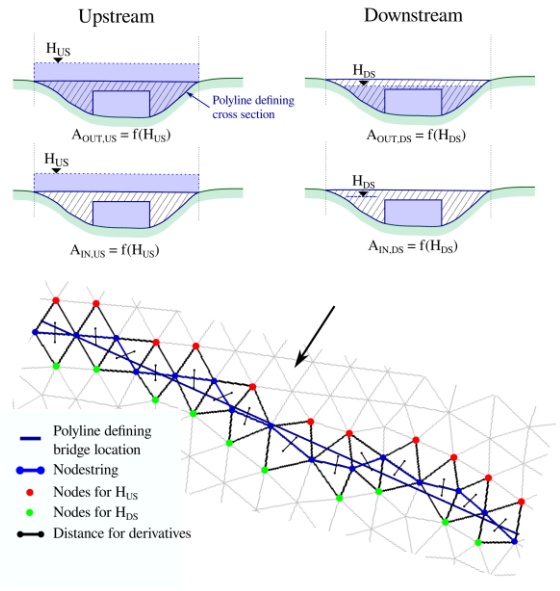

Figure 4. Implementation detail for a real case

III. VALIDATION CASE

The bridge module was validated through an experimental study conducted by [5]. The study was carried out in a 0.24 m wide and 6.0 m long laboratory flume. The bottom roughness in the flume was reported to be $n = 0.011\ s/m^{1/3}$. The experimental study encompassed a wide range of different bridge geometries, orientations to the flow and hydraulic boundary conditions, resulting in a total of 207 measurement points. The head losses exerted by the bridge structures were quantified by measuring the water levels upstream and downstream of the bridges. Upstream measurements were performed at a distance of 1.0 m from the bridge, while downstream measurements were taken at a distance of 3.0 m.

To validate the bridge module, we replicated the measurements numerically. Due to data availability, we considered 176 of the 207 experimental cases for validation. In the numerical model, the channel was expanded upstream to minimize the influence of the upstream boundary condition. For each case, the measured discharge was imposed at the upstream boundary and the measured water depth was prescribed at the downstream boundary. The bridge geometries were implemented as described in the prior sections of this paper. The simulations were run until steady state conditions were reached and the simulated upstream water level was compared to the measured one. The numerical model setup is illustrated in Figure 5.

Prior to validating all 176 experimental cases, we tested if the implementation is mesh independent. To do this, we compared the results obtained from simulations using the original mesh to simulations with a much finer computational grid. The original spatial resolution in longitudinal direction was about 0.1 m, whereas the resolution of the finer grid was around 0.025 m. The observed differences between the modelling results showed to be dependent on the specific case. However, the maximum observed difference in the water levels was merely around 1.5 %.

Figure 6 presents a comparison between the measured and simulated water depths for all 176 investigated cases (indicated by blue crosses). Overall, the head losses could be replicated well by the numerical model, yielding a coefficient of determination of $R^2 = 0.962$. This value is comparable to the results of [5], who reported statistics of 0.934 for their Borda-Carnot approach, 0.991 for their Borda-Carnot approach including a calibration coefficient and 0.953 for simulations performed with HEC-RAS. In Figure 6, several data points exhibit higher measured water levels compared to the simulated values. This phenomenon was also observed in the Borda-Carnot implementation of [5]. Contrary to that, the HEC-RAS simulations demonstrated less systematic underprediction of the head losses. We found that the Borda-Carnot based formulations tended to underestimate the energy losses for partly and fully submerged bridges, particularly when lower water levels were present downstream of the bridge (see Figure 1, Case 2a)

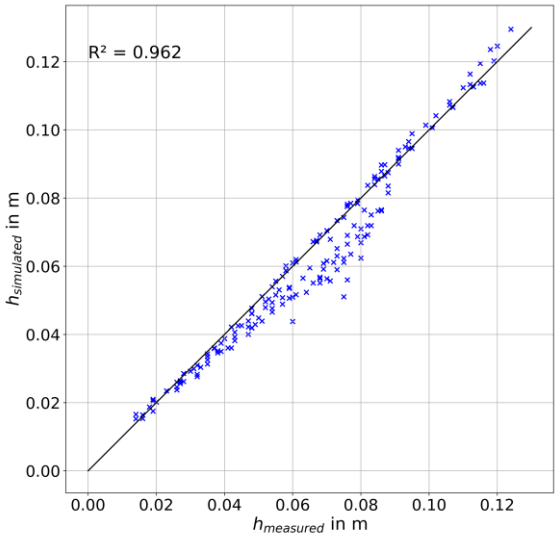

Figure 6. Comparison between simulated and observed upstream water depths for all 176 test cases (indicated by blue crosses)

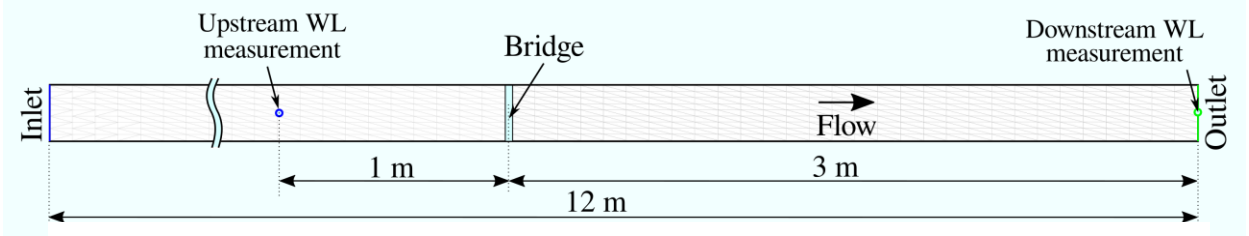

Figure 5. Setup of the numerical experiment, plan view

IV. User Example

A. Setup of the user example

This section demonstrates the implementation of multiple bridges for a generic test case. The test case was set up with one inlet and two outlet boundaries. The computational grid consisted of a total of 86,420 unstructured triangular elements with a mean edge length of about 1 m. The bottom elevations ranged from 0 to 16.2 m and the area of the study domain was about 60,000 m². The simulation was driven with a constant discharge of 30 m³/s until steady state conditions were reached. The study included three bridges with different cross sections. The elevations of the computational grid, the inlet and outlet boundary conditions and the locations of the three bridges are illustrated in Figure 7. This test case is meant to demonstrate the usage of the bridge module and is available on GitHub: https://github.com/tuggegese/T2D_BridgeModule

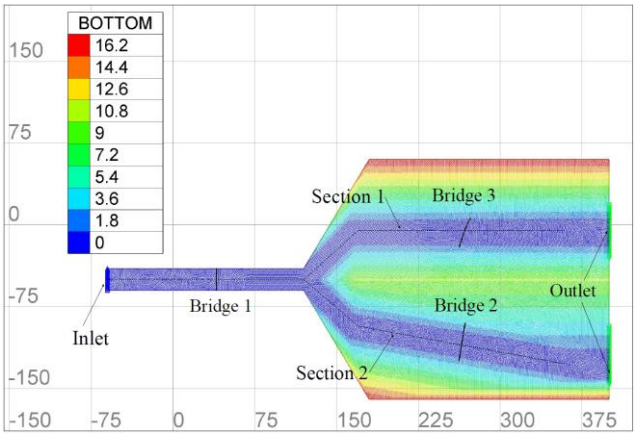

Figure 7. Overview of the example case, its bottom elevations and the locations of the bridges and longitudinal sections

For implementing the bridges, we first created two BlueKenue line sets. The first polyline was of the type “Open Line” and defined the location of the bridges in the computational grid (see Figure 7). This set of polylines was called “bridges.i2s” and was defined in the steering file by adding the following keyword: BRIDGE LOCATION FILE = ‘bridges.i2s’.

The next step was to resample the polylines defining the locations of the bridges. Afterwards, the bottom elevations were mapped to the lines and the resulting cross sections were saved in the ‘.xy’ data format. Converting the ‘.xy’ data sets to ‘.i2s’ allowed for loading the bottom cross sections of the bridges into the 2D canvas of BlueKenue. Subsequently, the cross sections of the bridges were drawn with polylines of the type “Closed Line”. The resulting cross sections of the bridges (dark blue polyline) and the extracted cross sections of the bottom elevations (red line) are shown in Figure 8. All three bridges were added to a single ‘.i2s’ line set, which was added to the steering file by setting the following keyword: BRIDGE SECTION FILE = 'bridgesCS.i2s'.

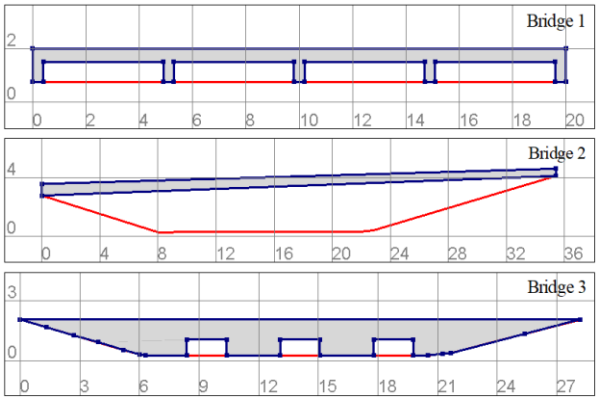

Figure 8. Cross sections of the three bridges (dark blue line) and bottom elevations (red line) in the study domain. The polylines are visualized in the 2D canvas of Blue Kenue

Besides the location and section files, the bridge module requires defining the number of implemented bridges, which was done in the steering file by adding the following keyword: NUMBER OF BRIDGES = 3.

B. Results of the test case

Figure 9 displays the simulated free surface elevations for the presented test case. Specifically, upstream water levels at the three bridge cross sections (B1, B2 and B3) and the free surface elevations along two longitudinal sections (S1 and S2, see also Figure 7) are visualized. The figure includes simulated water levels with and without considering the added head losses of the bridge structures, shown with blue and red lines, respectively.

Upon considering the effects of the bridges, we observed increases in the upstream water levels as follows: 0.11 m for Bridge 1, 0.02 m for Bridge 2, and 0.16 m for Bridge 3, respectively. Notably, the water level difference for Bridge 2, which did not come in contact with water, resulted from the backwater effects of Bridge 3. For the here presented case, the model computed contraction coefficients of 0.58 for Bridge 1, 1.0 for Bridge 2 and 0.34 for Bridge 3, by utilizing Equation 3 with the calibrated coefficients. For Bridge 1, the contraction coefficient was found to be in close agreement with the constant value of 0.62 suggested by [5]. As for Bridge 2, the presence of equal areas below and outside of the bridge led to a contraction coefficient of 1.0, effectively resulting in the contraction losses becoming zero, as evident from Equation 2. For the third bridge, Bridge 3, the contraction coefficient became quite small, allowing the consideration of additional energy losses due to the very small unobstructed flow area.

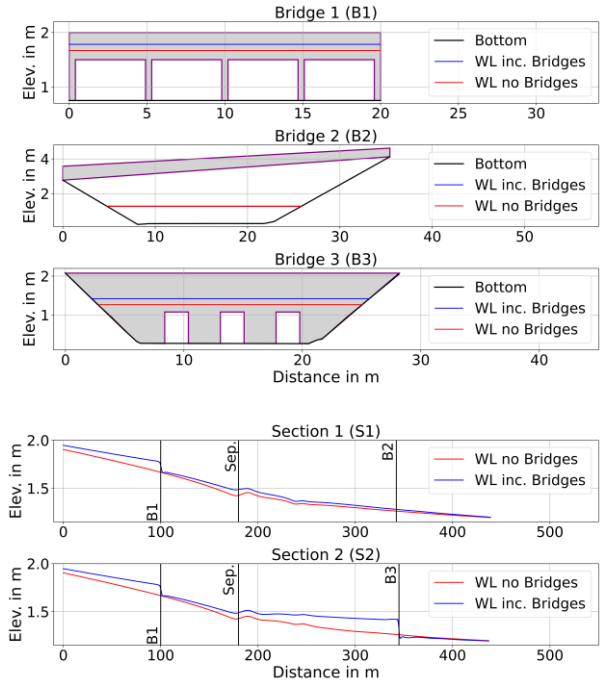

Figure 9. Results of the generic test case. Shown are the water levels (WL) with and without considering the backwater effects of the bridges upstream (US) of three bridge sections (B1, B2 and B3) and along two longitudinal sections (S1 and S2).

V. Discussion and Conlusion

The bridge module presented here was developed with the objective of providing a user-friendly method to consider backwater effects of both unsubmerged and submerged bridges with minimal user-defined parameters. To achieve this, we adopted a head loss based approach that relies solely on geometrical relationships and hydrodynamic flow properties at the bridge structure.

Our investigations and also the study conducted by [5] showed that the traditional Borda-Carnot approach, commonly used for pipe flows, underestimates the total energy losses imposed by the bridge structure on the flow, particularly when the bridge deck became submerged, leading to pressurized flow conditions. This underestimation could be attributed to the more irregular geometries of real bridges compared to pipes, as well as additional 3D hydrodynamic effects that cannot be accurately captured by contraction and expansion losses alone.

In an attempt to account for these additional losses, [7] proposed a constant multiplication factor of 1.31 for the contraction losses. On the other hand, [5] used a dynamic calibration factor, dependent on the Froude numbers upstream and downstream of the bridge, the ratio of the occluded area, and a constant describing the bridge regime (unsubmerged, partially submerged, or fully submerged). We observed that a constant calibration factor, as suggested by [7], failed to accurately represent the additional losses for all test cases. Similar to [5], we thus opted for a dynamic calibration parameter that increased the computed energy loss in proportion to the blocked area. Consequently, a more occluded cross section would result in significantly higher head losses compared to a barely submerged bridge.

To address this, we calibrated the head losses using the contraction coefficient and employed Formula 3 as a starting point. This formulation offered the advantage of yielding higher losses as the flow area became more obstructed and also resulted in a head loss of zero when the bridge did not come in contact with water (see Formula 2). This adapted approach for computing the contraction coefficient produced satisfactory results for the validation case. In the user example, this led to contraction coefficients of 0.58 for Bridge 1, 1.0 for Bridge 2, and 0.34 for Bridge 3, respectively. For reference, [5] used a constant contraction coefficient of 0.62.

To conclude, we can give the following remarks and suggestions, when applying this approach for modelling unsubmerged and submerged bridges:

- The algorithm works well for a wide range of flow conditions, however, during high flow conditions the standard Borda-Carnot equation tends to underestimate the energy losses exerted by the bridge structure. Although we introduced a dynamic calibration coefficient, it may be necessary to perform additional calibration for each individual case.
- Our investigation reveals that the proposed module remains largely stable when the underlying hydrodynamics are stable. This emphasizes the importance of considering the overall hydrodynamic conditions to ensure the model's reliability and robustness.
- During our simulations, we observed minimal slowdown when incorporating the bridge structures (at least with three bridges). This demonstrates the computational efficiency of the proposed approach, making it a practical choice for large-scale applications.

Acknowledgement

We like to thank our colleagues from “Niederer and Pozzi” (www.nipo.ch) for testing the here presented bridge module. We also express our gratitude to the independent reviewer.

References

[1] T. Picel, A. Havlik, D. Mattas and K. Mares, “Hydraulic calculations of bridges at high water stages” in Journal of Hydraulic Research, vol. 45, Taylor & Francis, pp. 400-406, 2007.

[2] Hydrologic Engineering Center, “HEC-RAS 2D user’s manual”, U.S. Army Corps of Engineers, Davis CA., 2023.

[3] Hydronia LLC, “RiverFlow2D Reference Manual”, March 2023

[4] Hydrotec Ingenieurgesellschaft für Wasser und Umwelt mbH, “Hydro-AS-2D Benutzerhandbuch“, Aachen, Germany, version 5.1.5, september 2019

[5] H. Ratia, J. Murillo and P. García-Navarro, “Numerical modelling of bridges in 2D shallow water flow simulations”, in International Journal for Numerical Methods in Fluids, Wiley, 75:250-272, 2014

[6] VT. Chow “Open Channel Flow” MacGraw-Hill Book Co. Inc, New York, 1959

[7] D. Aigner and G. Bollrich, “Handbuch der Hydraulik für Wasserbau und Wasserwirtschaft“, 2nd Edition, Beuth Verlag GmbH, Berlin Germany, 2021

[8] H. Oertel, L. Prandtl, M. Böhle, K. Mayes, “Prandtl’s Essentials of Fluid Mechanics“, Springer, 2004